ESA Project **METHANE+**	**Scientific Assessment Report**	Version: 2.0 Doc ID: SAR-D8-CH4PLUS Date: 9-March-2023

Scientific assessment report

ESA project METHANE+ led by SRON

Task 3, WP 3000, Deliverable 8 (D8)

Lead author:
Sander Houweling (VU)
Co-authors:
Jacob van Peet (VU), Julia Marshall (MPI-BGC),
Tonatiuh Guillermo Nuñez Ramirez (MPI-BGC)

Change log

Version	Date	Status	Authors	Reason for change
0.1	17-June-2022	Draft	see title page	New document
1.0	15-July-2022	Version for review by ESA	see title page	First round of corrections + contribution DLR
2.0	9-March-2023	Corrected to address ESA's comments		Comments and corrections raised by ESA

Authors

Vrije Universiteit Amsterdam (VU), Amsterdam, The Netherlands

- Sander Houweling
- Jacob van Peet

Max Planck Institute for Biogeochemistry (MPI-BGC), Jena, Germany:

- Julia Marshall (currently at DLR)
- Tonatiuh Guillermo Nuñez Ramirez

Table of Contents

1. Executive summary 5
2. Objectives and structure 6
3. Inversion methods and implementation of TROPOMI and IASI 7
   3.1. TM5-4DVAR 7
      3.1.1. General inversion setup 7
      3.1.2. Implementation of TROPOMI data 7
      3.1.3. Implementation of IASI data 9
      3.1.4. Implementation of joint TROPOMI-IASI data 10
      3.1.5. OH optimization 11
   3.2. Jena CarboScope (DLR) 11
      3.2.1. General inversion setup 12
      3.2.2. Implementation of TROPOMI data 12
      3.2.3. Implementation of IASI data 14
4. Inversion results 15
   4.1. Comparison of results using different retrieval datasets 15
      4.1.1. TM5-4DVAR 15
      4.1.2. Jena CarboScope (DLR) 20
   4.2. The combined use of TROPOMI and IASI data 22
      4.2.1. Fit residuals: SWIR-TIR vs single instrument inversions 22
      4.2.2. Comparison of 3-year inversions in TM5-4DVAR 25
      4.2.3. Regional benefits of joint SWIR-TIR retrievals 28
   4.3. Validation with independend measurements 31
      4.3.1. TM5-4DVAR 31
      4.3.2. Jena CarboScope (DLR) 32
5. Summary and recommendation for future work 35
6. References 37

1. Executive summary

This report documents the development of the TM5-4DVAR and Jena CarboScope inverse modelling systems in the Methane+ project. Both systems have been prepared for the use of the new satellite retrievals of total column methane (XCH4) from TROPOMI and IASI that are made available in the project. Inversions have been performed using these datasets and the resulting global CH_4 emissions estimates are presented and compared in this report.

The focus is on the combined use of XCH4 retrievals from TROPOMI and IASI, either using both datasets in a single inversion or using joint SWIR-TIR retrievals, and the added value that this approach can bring for estimating surface emissions. An important limitation of many operational inversion systems, including the operational CH_4 reanalysis of the Copernicus Atmosphere Monitoring Service (CAMS), is that they do not optimize methane sinks. The question is whether the combined use of TROPOMI and IASI data is sufficient to constrain CH_4 sources and sinks independently. To assess this, the TM5-4DVAR system was modified for the joint optimization of methane sources and sinks. To apply this new capability, we have extended our inversion time window to cover the full year of 2020. Doing so allows us to investigate the role of sources and sinks in the sharp methane increase observed in 2020.

Our new inversions using TROPOMI and IASI yield consistent emission adjustments compared to the common set of a priori fluxes. Results are consistent also with the surface measurements network, indicating that our setups account for any obvious systematic errors in the transport models and satellite data. Our inversions attribute the accelerated global CH_4 increase in 2020 to emissions or sinks depending on the dataset that is used in the inversion. This indicates that the datasets have different sensitivities to the two components. This is a promising finding that is worth investigating further, for example, by exploring the degrees of freedom that are assigned to the sink.

The joint SWIR-TIR retrieval of CH_4 sub-columns is a promising approach, but its use in inverse modelling requires further attention. So far, our attempts to apply this dataset to TM5-4DVAR yielded poorer comparisons to independent data (surface and TCCON) than the use of separate TROPOMI and IASI retrievals for reasons that were not yet elucidated.

2. Objectives and structure

This deliverable report documents the activities in Methane+ WP3000 on the scientific analysis of retrieval datasets that are generated in the project. This analysis makes use of two inverse modelling systems (TM5-4DVAR and Jena CarboScope) that have been further developed in WP3000 to process the new retrieval datasets.
All global inversions have been performed for a period of at least two years (April 2018 – April 2020), as was initially proposed. These simulations will be referred to as the 2-year inversions in the following. In addition, a subset of inversions has been performed for an extended period covering the full year of 2020, referred to as the 3-year inversion. This extension was motivated by the exceptionally strong global growth rate of CH4 that was observed during 2020, raising questions about the underlying causes that we were hoping to answer using the satellite data sets prepared in Methane+. Table 1 provides an overview of retrieval datasets that were processed in TM5-4DVAR and Jena CarboScope for the two time windows. The TM5-4DVAR framework has been modified for optimizing CH4 sinks in addition to emissions. This code has only been applied to the extended time window, because it became available only towards the end of the project and because of the interest in using this code to assess a possible contribution of changing sinks to the increased CH4 growth rate.

Table 1: Inversions performed in WP3000.

Retrieval dataset	Time window	Inverse model	TM5-4DVAR OH optimization
Surface network	201801 - 202006	TM5-4DVAR & CarboScope	-
S5p Operational	201801 - 202006	TM5-4DVAR & CarboScope	-
S5p SRON v16_14	201801 - 202006	TM5-4DVAR & CarboScope	-
S5p WFMD v1.2	201801 - 202006	TM5-4DVAR	-
S5p WFMD v1.5	201801 - 202006	CarboScope	
IASI LMD v9.1	201801 - 202006	TM5-4DVAR & CarboScope	-
IASI RAL v2	201801 - 202006	TM5-4DVAR & CarboScope	-
Surface network	201801 - 202103	TM5-4DVAR & CarboScope	+
S5p SRON v18_17	201801 - 202103	TM5-4DVAR & CarboScope	+
IASI RAL v2	201801 - 202103	TM5-4DVAR & CarboScope	+
S5p SRON & IASI RAL	201801 - 202103	TM5-4DVAR & CarboScope	+
Joint SWIR/TIR retrieval	201801 - 202103	TM5-4DVAR & CarboScope	+

This report will continue with a description of the two inverse modelling systems and the modifications that were made to prepare them for the use of new data, including the extension to OH optimization in TM5-4DVAR. Inversion results are presented in section 3, comparing global methane emissions optimized using different retrieval datasets and inversion setups. Here, the focus is on differences and similarities in results obtained using SWIR and TIR retrievals and the added value of their combined use. The two inverse modelling systems help to identify adjustments to the common a priori emission inventories that are robust to assumptions that are made in the inversion setup. Results for TM5-4DVAR are presented with and without optimization of the OH sink, to assess the independent constraints on methane source and sinks

provided by the data. The main outcomes and recommendations for next development steps in the development of satellite data-driven methane inversions are summarized in section 4.

3. Inversion methods and implementation of TROPOMI and IASI

3.1. TM5-4DVAR

3.1.1. General inversion setup

The standard setup of the TM5-4DVAR inverse modelling system that is used for the activities in WP3000 that are presented in this report has been documented in the Requirements Baseline Tech Note (D1) and will not be repeated here. The extensions that have been developed within Methane+ to be able to use the new satellite data products that are made available are described in this section. All other inputs are kept as close as possible to the TM5-4DVAR version that is used for the CAMS CH4 reanalysis. This way the results that are presented can be compared to the CAMS reanalysis, including inversions of GOSAT data that have not been repeated for Methane+. Any information regarding the standard setup can be found in the D1 report or the technical documentation of the CAMS CH_4 reanalysis (Segers and Houweling, 2020).

3.1.2. Implementation of TROPOMI data

To deal with the large volume of TROPOMI data, we cluster them in super-observations rather than assimilating each individual measurement as is done for GOSAT. Super-observations are averages of all data from a single satellite orbit that fall in the same model grid box.
To explain the use of super-observation and discuss possible implications, let us first consider the current treatment, without super-observations. In the conventional setup using GOSAT data, the following equation is used to introduce the averaging kernel in the sampling module of TM5-4DVAR,

$$XCH4_{mod} = A(p).CH4_{mod}(p) + (1 - A(p)).CH4_{prior}(p), \qquad (eq.\ 1)$$

with $XCH4_{mod}$ the model simulated total column, sampled as GOSAT, $A(p)$ the GOSAT column averaging kernel as function of the atmospheric pressure p, $CH4_{mod}(p)$ the modelled methane vertical profile at the location of a GOSAT retrieved XCH4 column, and $CH4_{prior}(p)$ prior CH_4 profile used in the retrieval.
In the case of super-observations, $XCH4_{mod}$ is the average of multiple TROPOMI measurements from the same orbit that fall into the same TM5 model grid box. The corresponding averaging kernel equation is,

$$XCH4_{mod} = \bar{A}(p).\overline{CH4_{mod}}(p) + \left(1 - \bar{A}(p)\right).\overline{CH4_{prior}}(p), (eq.2)$$

where the overbars denote weighted averages using the inverse retrieval uncertainty of individual measurements as weights, consistent with the averaging procedure that is used to compute super-observations from the TROPOMI data. Taking the mean averaging kernel introduces no error, since the model profile is the same for each retrieval in the super-observation. The same is true for the prior profile, since the operational processing uses a priori information from the CAMS reanalysis generated using TM5-4DVAR on the same grid. In our test simulation, an error is introduced by using a coarser resolution transport model than what is used for the TROPOMI prior (6°x4° instead of 3°x2°). However, this error is expected to be small, since the spatial distribution of a priori mixing ratios is quite smooth. The aim for the future is to increase the resolution of the CAMS reanalysis to 1°x1°. It is expected that the operational TROPOMI processing will not follow that resolution increase. This is not a problem, however, since errors are only introduced when the data are used in a model that has a lower resolution than the retrieval prior.
The method for dealing with the regridding between the vertical levels of TM5 and the TROPOMI retrieval is also different than what was used before for GOSAT. When the surface pressure of the data is higher than in the model, the original method was to "stretch" the model profile. This method is defensible for CO_2 but we changed it for CH_4 to avoid any possible influence on the vertical profile and notably the stratospheric bias between TM5 and satellite measurements that we are trying to solve. The new method takes the average mixing ratio of a few PBL layers for extrapolation of the mixing ratio from the modelled surface to the retrieved surface (which in this case is at *lower* surface elevation).
The data uncertainty of the super-observation is taken to be the standard deviation of the retrievals that a super-observation is composed of, which can be improved further in a later stage but is considered a reasonable and conservative starting point. The retrieval uncertainty that is contained in the L2 datasets only reflects the spectral fit, which was found to significantly underestimate overall retrieval uncertainty. The filtering of the data follows the general recommendations for the TROPOMI operational XCH4 retrieval product (Hasekamp et al, 2019). In addition, retrieval biases are corrected for as described and shown in the next section.

TROPOMI data are bias corrected in two ways: 1) using the bias corrected version of the data provided in the L2 retrieval data, 2) using a TM5-4DVAR derived bias correction. The second correction accounts for any inconsistencies between inversions using surface and satellite data that would cause the latter to deviate from the methane mixing ratio as observed in the remote marine background. As reported by Monteil at al. (2013) for inversions using GOSAT, this inconsistency can be restored by a applying a latitudinal correction to the satellite data. As pointed out by Locatelli (2015), this bias is likely not an actual error in the TROPOMI data but in atmospheric transport models, caused by inaccuracies in the representation of stratospheric transport in the model. To derive the correction the model is first optimized to surface data. Subsequently, the

optimized 3D methane mixing ratio field is sampled as the TROPOMI satellite would do, accounting for its vertical sensitivity as defined by the retrieval averaging kernel. The zonal mean difference between model simulated and actual TROPOMI data is evaluated in monthly 4° latitude bins, corresponding to the resolution of the transport model (see Figure 1). Mean biases are calculated for each month in the inversion time window and used as bias correction to the TROPOMI data in the inversion. This way we correct only the zonal mean latitudinal gradient accounting for its mean seasonality, but not for inter-annual variations.

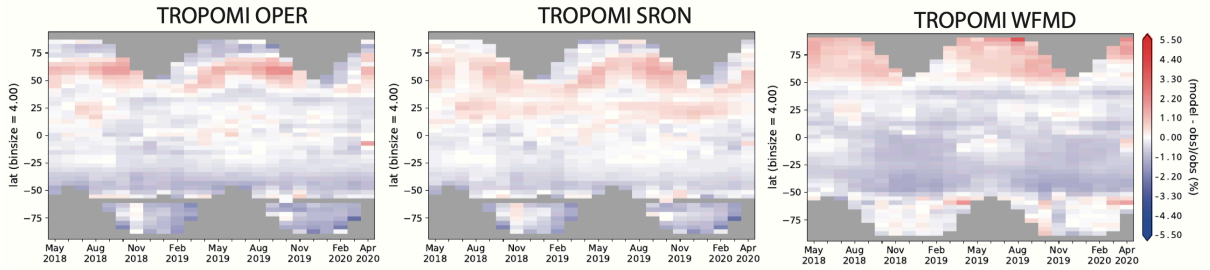

Figure 1: Monthly mean zonal difference between TROPOMI XCH_4 retrievals and TM5-4DVAR after optimization using surface data.

The bias shows a systematic north-south gradient. We can be confident that this is a bias rather than a useful signal of source/sink deficiencies in the model because the surface network provides a strong and accurate constraint on the north-south gradient of methane. The pattern repeats from one year to the next, justifying our approach of applying only a time averaged correction. Bias corrections look similar for the operational and SRON data, but somewhat different for WFMD. As mentioned earlier, the main cause is believed to be the stratospheric age of air in offline atmospheric transport models, but since the correction varies between retrieval versions it must have a contribution from retrieval error also.

3.1.3. Implementation of IASI data

The implementation of RAL IASI follows the same logic as explained for TROPOMI in section 3.1.2. Despite the use of a profile retrieval, we only use retrieved total columns in our inversions. For LMD IASI, which is a total column retrieval, the averaging kernels represent the weights of each vertical layer in column average. Bias corrections for the IASI retrievals have been computed using the same method as used for TROPOMI (see section 3.1.2). The uncertainty of IASI super-observations is taken to be the weighted average of the individual retrieval uncertainties.

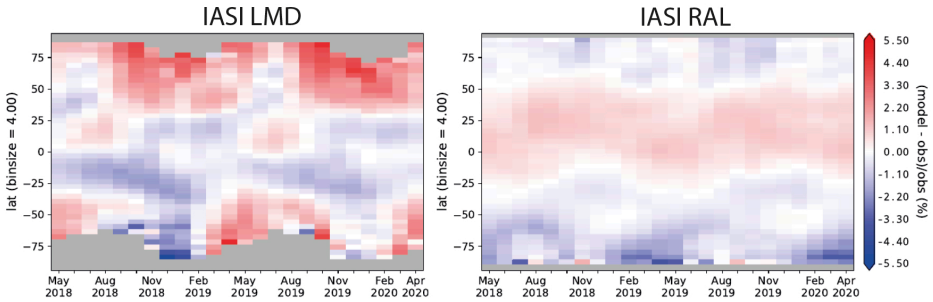

Figure 2: Monthly mean zonal difference between IASI XCH_4 retrievals and TM5-4DVAR after optimization using surface data.

The zonal mean bias corrections for IASI (Figure 2) look very different from those for TROPOMI, which could be explained by the difference and vertical sensitivity between the TROPOMI and IASI retrievals. However, the LMD and RAL bias corrections also look very different, pointing to an important contribution from the retrieval. An important contribution to RAL bias turned out to be an inaccuracy in the representation of stratospheric N_2O, which has been corrected in the v3 retrieval.

3.1.4. Implementation of joint TROPOMI-IASI data

For the combined use of IASI and TROPOMI in the 3-year inversions, the bias correction for each product is applied. In this case the inversion reads in the same TROPOMI and IASI super observations, following the same procedure as used in the inversions using data from a single satellite. For the joint TROPOMI-IASI retrieval, data are available for the full column as well as the tropospheric and stratospheric sub-columns. The bias correction for the full column and 0-6 km sub column are shown in Figure 3. The remainder of this report focuses on the use of the 0-6 km sub column, which brings the most useful information in addition to the combined use of TROPOMI and IASI in a single TM5-4DVAR inversion.

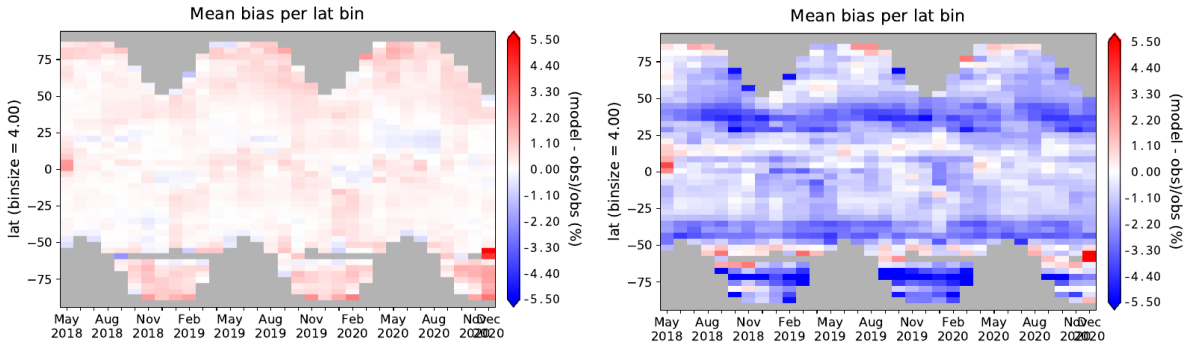

Figure 3: Monthly mean zonal difference between joint TROPOMI-IASI XCH4 retrievals and TM5-4DVAR after optimization using surface data for the total columns (left panel) and for the 0-6 km sub columns (right panel).

As can be seen, the latitudinal dependence of the total column product is very small. Larger offsets are seen in the 0-6 km product, but the pattern looks different from TROPOMI and IASI retrievals in a way that cannot easily be explained from the separate data products.

3.1.5. OH optimization

The optimization of the atmospheric sink of methane has been implemented in TM5-4DVAR as scaling factors of the default OH field that is used in inversions that do not optimize OH. The setup allows optimization of annual OH factors for all latitudinal bands of the TM5 model. However, the inversions presented in section 4 only use global annual scaling factors, with a methyl-chloroform-derived *a priori* value of 0.92 that is used also in inversions without OH optimization, and an *a priori* uncertainty of 20%.
The implementation of OH optimization in TM5 is analogous to the optimization of emissions, except for the location in the code where the methane sink is applied. In forward simulation this part of the code represents the formula:

$$CH4(t_1) = CH4(t_0) - f_{OH}.k_{CH4OH}.OH.CH4(t_0).dt \qquad \text{eq.3}$$

where k_{CH4OH} is the temperature-dependent rate constant of the chemical reaction between CH_4 and OH during timestep $dt = t_1 - t_0$. Here f_{OH} is the scaling factor of OH that is optimized in the inversion. For the corresponding emission equation, the second term on the right hand side is $E.(t_1 - t_0)$.
In the adjoint model, the adjoint equivalent of equation 3 is:

$$Adf_{OH,t2} = adf_{OH,t1} - k_{CH4OH}.OH.CH4.dt.adCH4 \qquad \text{eq.4}$$
$$AdCH4_{t2} = adCH4_{t1} - f_{OH}.k_{CH4OH}.OH.dt.adCH4 \qquad \text{eq.5}$$

where adCH4 and adf_{OH} are the adjoint sensitivities of the active variables CH4 and f_{OH}. To compute adf_{OH} requires $CH4(t_0)$ to be available to the code. Since the adjoint model propagates in the reverse time direction, $CH4(t_0)$ cannot be computed. The method to solve this is to store the 3D CH4 field at every time step of the forward model simulation and read it from file in the adjoint simulation. Note that in the adjoint simulation, t_0 is at the end of timestep dt that starts at t_1. Therefore, at t_1 a CH4 field is read from file that corresponds to t_0.
After coding the adjoint model, its consistency with the forward model is tested using the adjoint and gradient tests. In the TM5-4DVAR implementation the adjoint test only tests the validity of the adjoint TM5 model, whereas the gradient test also covers the code that uses the output of TM5 to compute the cost function value.

3.2. Jena CarboScope (DLR)

3.2.1. General inversion setup

The Jena CarboScope (Rödenbeck, 2005) is a Bayesian inversion framework that estimates trace gas surface fluxes given the constraints of their observed atmospheric mole fraction combined with atmospheric transport. The inversion model is based around the offline chemistry transport model TM3 (Tracer Model 3, Heimann and Körner, 2003). The transport simulations are run at a resolution of 3.8° latitude and 5° longitude, with 26 vertical levels.
Prior fluxes representing different surface processes are decomposed into different frequency components (e.g. long-term trend, seasonal, interannual, high-frequency), resulting in a statistical flux model. The temporal and spatial correlation lengths and the prior uncertainty can be defined for each of these components separately.
In this case, four separate processes are included in the optimization, using input consistent with the CAMS inversions and distributed by VU within the project. These processes are wetland emissions, rice emissions, biomass burning, and “other”, which captures most anthropogenic activities, including fossil fuel-related activities, agriculture, and waste.
Unlike the innovations developed within the project for the TM5-4DVAR modelling system, the methane sink is not optimized in this model. There are other differences in the setup, such as the algorithm used to minimize the cost function, which is linear. As such, non-physical negative methane fluxes may occur for some pixels at times. In general, these negative fluxes are cancelled out when integrating over a larger region.

3.2.2. Implementation of TROPOMI data

The preprocessing of the TROPOMI data for use in the model was similar to that outlined in Section 3.1.2 for the TM5-4DVAR system: All good retrievals per doxel (model gridbox per orbit) were aggregate to form a super-observation. The mean value for XCH_4 was taken, with values inversely weighed by the reported measurement precision. To balance the mismatch in the scale of the reported measurement uncertainties between the various retrievals (with the WFMD retrievals reporting uncertainties nearly a factor of 10 higher), the uncertainty per super-observation was defined as either the the standard deviation of all soundings within the doxel, or double the mean precision, whichever was larger.
In order to make inversion results based on surface measurements comparable with those using total-column measurements, a model-specific bias correction was applied. The default approach used in the CarboScope system is a second-order polynomial as a function of latitude and month, following Bergamaschi et al. (2007), namely:

$$XCH_{4,corrected} = XCH_{4,measured} - \sum_{n=0}^{2} a_n(t) lat^n \qquad \text{eq. 6}$$

To find the parameters a_0, a_1, and a_2 per month (time t), first an inversion using only surface-based measurements is carried out. In the case of this study, this is a network of 31 stations, primarily background sites. Once these fluxes have been optimized, a forward simulation is carried out during which the atmosphere is sampled according to

the time and location of the (aggregated) satellite measurements, taking into account the (mean) averaging kernel and prior profile provided with the retrieval. The difference between the measurements and the simulated concentrations per month is then fit to determine the parameters as a function of latitude.
This results in a rather smoothly varying correction, by definition. This is consistent with the sorts of errors that might be the result of errors in the representation in the stratosphere, which would have a similar zonal structure and seasonal cycle. However, this does not account for some differences at high latitudes which were found to have much more structure, with differences between the SRON retrievals and the fields from the surface-based inversion often showing a zig-zag feature north of about 50°, particularly in the Northern Hemisphere spring. It is hypothesized that this might be the result of retrieval errors over snow cover. The difference between the surface-station-optimized fields and the WFMD TROPOMI retrievals is comparatively smooth. An example of this is shown in Figure 4.

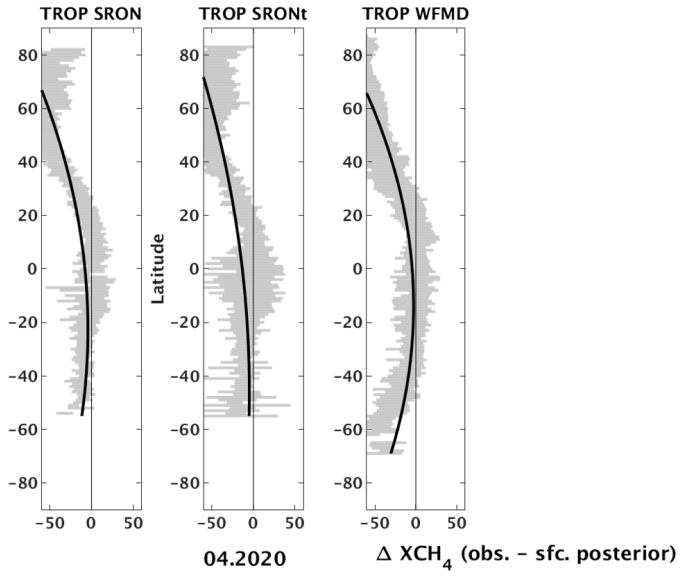

Figure 4: Zonal structure of the difference between three different retrieval products and the surface-based inversion of the Jena CarboScope for April 2020. On the left is the SRON operational product, in the middle is the "scientific" product, and on the right is the WFMD retrieval, corresponding the second, third, and fourth entries in Table 2, respectively. The 2nd-order polynomials are shown as thick solid lines. The grey bars represent the standard deviation of the measurements per 1° latitudinal bin.

The structure seen in this difference is consistent with the results in the TM5-4DVAR comparison shown in Figure 1. In order to test the impact of a more granular bias correction approach, a similar mean difference per monthly latitudinal bin was also tested. The resulting (additive) bias corrections SRON v18 product and the WFMD v1.5 product are shown in Figure 5. Note that in this figure the bias is plotted as the obs – model difference, whereas biases for TM5-4DVAR were presented as model – obs.

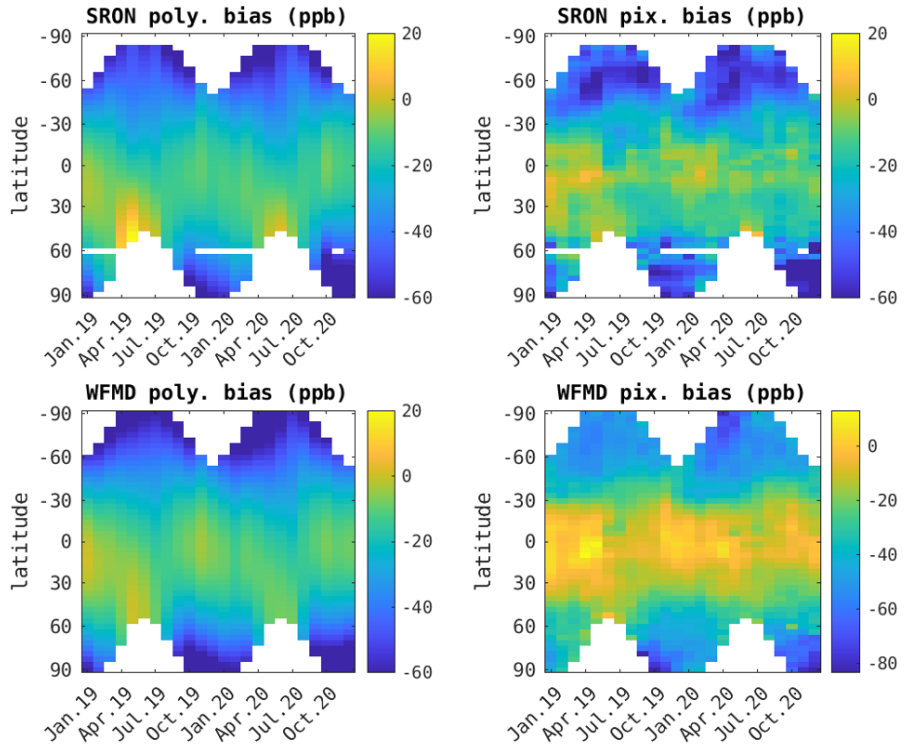

Figure 5: Two methods of bias correction tested here, the 2nd-order polynomial on the left, and the latitudinal-pixel-based method on the right. The upper row is for the SRON v17 product, the bottom row is the WFMD v1.5 retrieval.

3.2.3. Implementation of IASI data

Essentially the same procedure was followed for the implementation of the IASI retrieval products. For the joint SWIR-TIR retrieval from RAL, only the 0-6 km sub-column was tested, as this raises the possibility of not requiring as much ad hoc bias correction due to its theoretical insensitivity to the model's representation of the stratosphere. The two versions of the bias correction were fit for the IASI products as well, as is shown in Figure 6.

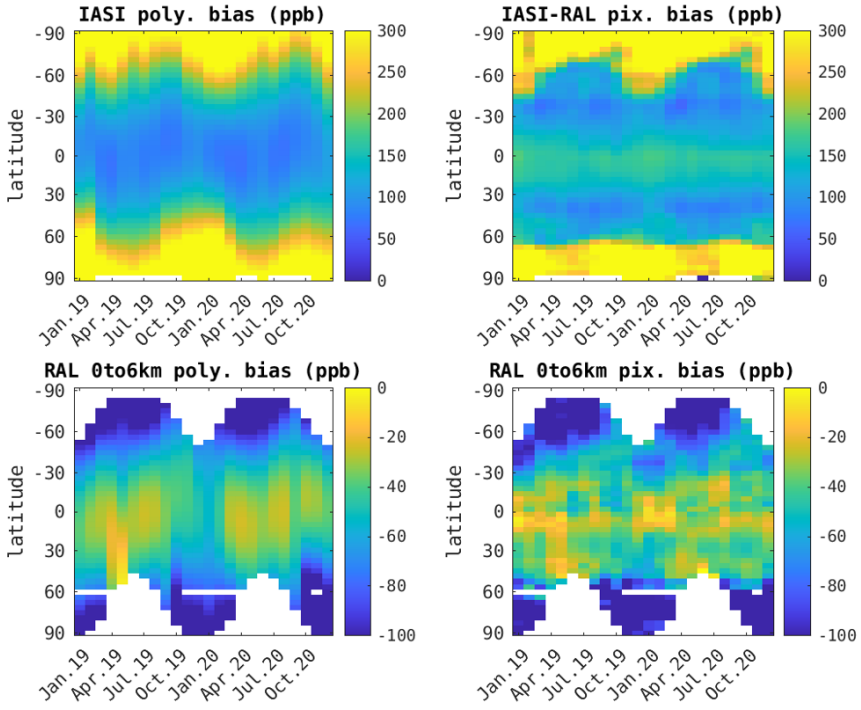

Figure 6: As in Figure 5, but for the RAL IASI retrieval (upper row) and the 0-6 km sub-column of the joint SWIR-TIR retrieval (bottom row).

Initially, it was only planned to use the Jena CarboScope to provide forward-modelling-based analysis of the IASI retrievals. This choice was made because it was clear that the model did a poor job of representing the upper troposphere and lower stratosphere, as can clearly be seen with the large, structured biases in the top panel of Figure 6. These are much more severe than the biases seen in the TIR products in the TM5-4DVAR model in Figure 2. Interestingly, the structure in the biases for the 0-6 km sub-column is much more similar between the two models. Nonetheless, some inversion modelling was attempted as well, as reported in Section 4.1.2.

4. Inversion results

4.1. Comparison of results using different retrieval datasets

4.1.1. TM5-4DVAR

For TM5-4DVAR, the 2-year inversions are used to compare results that are obtained using different retrieval datasets. As a first performance test for the TM5-4DVAR inversions, the fit residuals have been analysed before and after optimization (Figure 7 for Tropomi and Figure 8 for IASI).

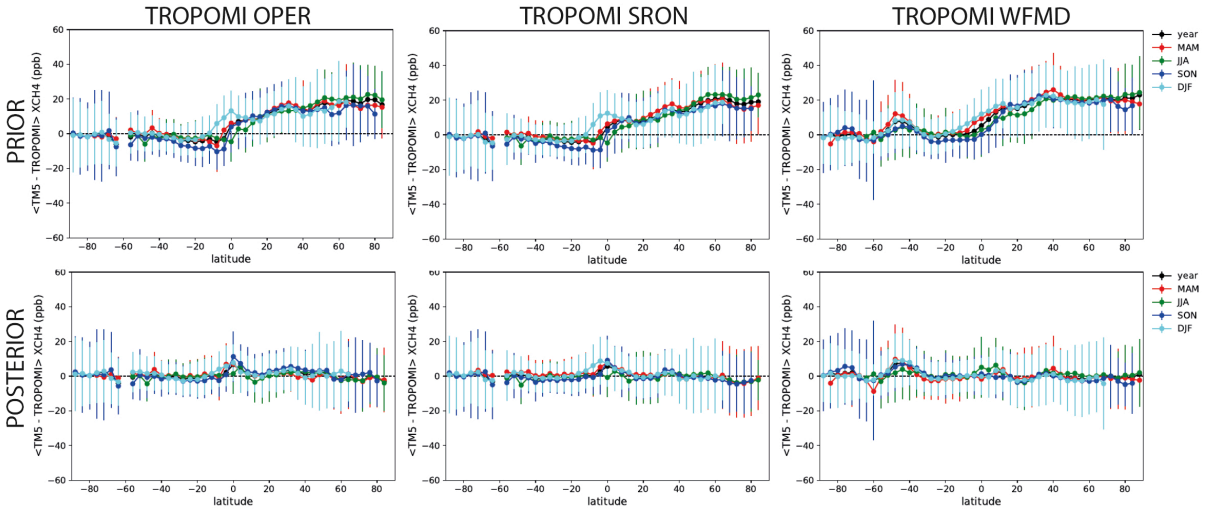

Figure 7: Comparison of zonal and seasonal mean fit residuals between TM5-4DVAR and Tropomi data before (prior) and after (posterior) inversion optimization. Error bars represent the standard deviation of the variation within each latitude bin.

Overall, the optimized results are as expected, without any significant systematic differences between optimized model and data. The largest deviations show up in latitude bins where the number of available data is less and/or retrievals uncertainties are larger. This applies the most to the high latitudes of the southern hemisphere due to low surface albedo over sea and ice. The influence of the seasonal availability of sunlight is also visible at the high latitudes of the southern and northern hemisphere. The standard deviation of the fit residuals varies around 1% of total column methane, as expected for the combined model and retrieval uncertainty.

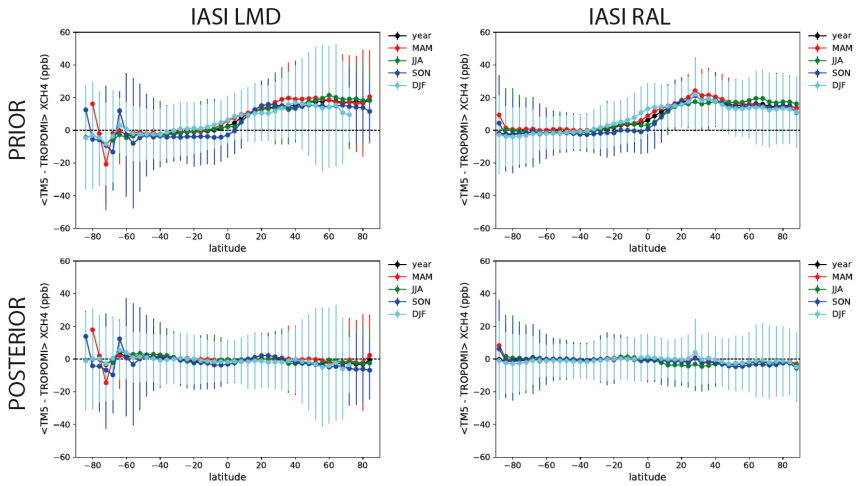

Figure 8: As Figure 7 for IASI data.

A next step in the evaluation of inversion results is to compare the optimized model state with surface measurements (see Figure 9). If the inversion improves the fit to

surface stations compared with the prior, then the inner circle has a lighter colour than the outer ring. As can be seen, this is the case for most of the inversions, with comparable performance between them. The inversion using IASI LMD shows somewhat larger residuals in the remote southern hemisphere than the other inversions.

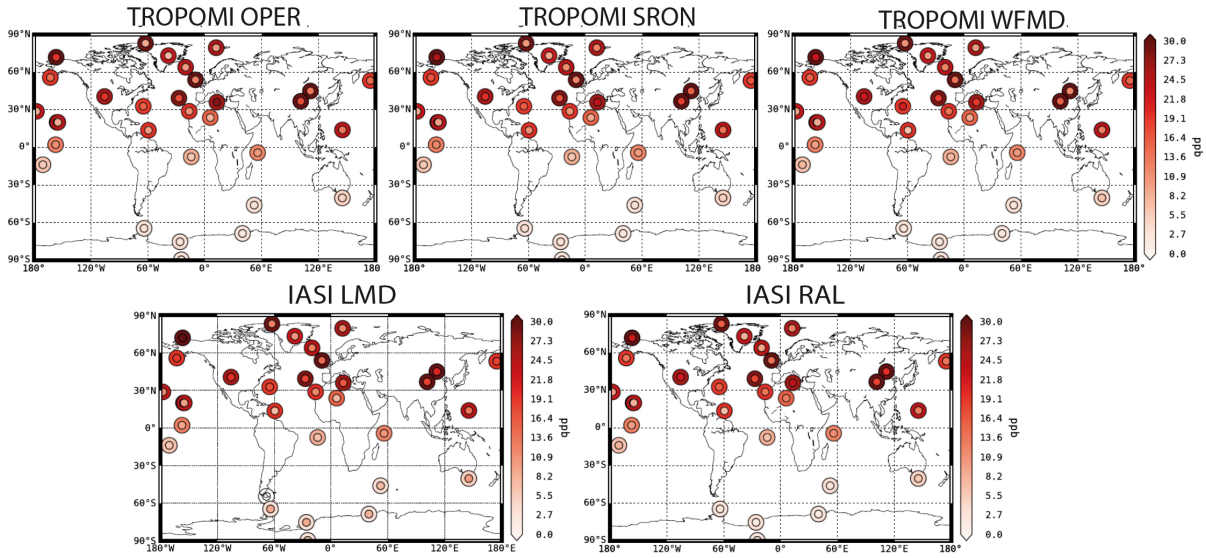

Figure 9: Fit residuals between TM5 and surface measurements. Outer rings represent the RMSE between measurements and the a priori model, inner circles that of measurements and the *a posteriori* model.

Comparing results with (Figure 9) and without (Figure 10) bias correction convincingly demonstrates the improved performance that is obtained using the bias correction. This difference is most notably for the measurement stations in the southern hemisphere.

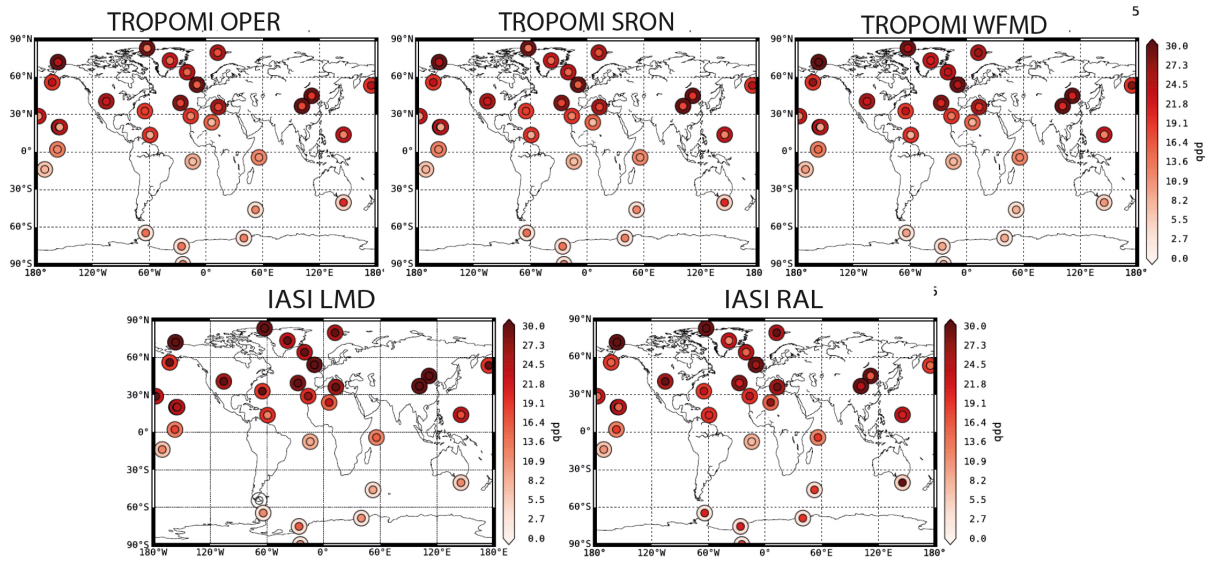

Figure 10: As Figure 9 for inversions without bias correction.

Gridded maps of inversion-optimized fluxes are shown in Figure 11. The fluxes are expressed as annual fluxes and represent the mean over the time window of the inversion minus 3 month's spin-up and spin-down (i.e. the two-year period from 2018-05-01 until 2020-05-01). The differences between prior and posterior (right column) is the most informative about the impact of the atmospheric measurements on the fluxes and difference that are found using different datasets. All inversions reduce the emissions over south-east Asia, but to a varying extent and with a varying attribution of this decrease between China and India. It is useful to also include the Middle East in this comparison. The Asian band of emission reductions is compensated by emission increases over the Tropics and the mid latitudes of the Northern Hemisphere. Regional differences occur, but the general pattern is fairly consistent between the inversions.

The surface inversion reduces emissions from China, India and the Middle East. All inversions increase the emission over the Middle East relative to the surface inversion, except for IASI RAL. The SRON TROPOMI retrieval shows less emission reduction over India and China than the surface inversions. Comparing the results in the left panel it becomes clear that the adjustments represent a significant fraction of the total emissions over these countries. The IASI LMD inversion puts most of the emission reduction over China, whereas IASI RAL moves it westward to India and the middle East compared with the TROPOMI inversion.

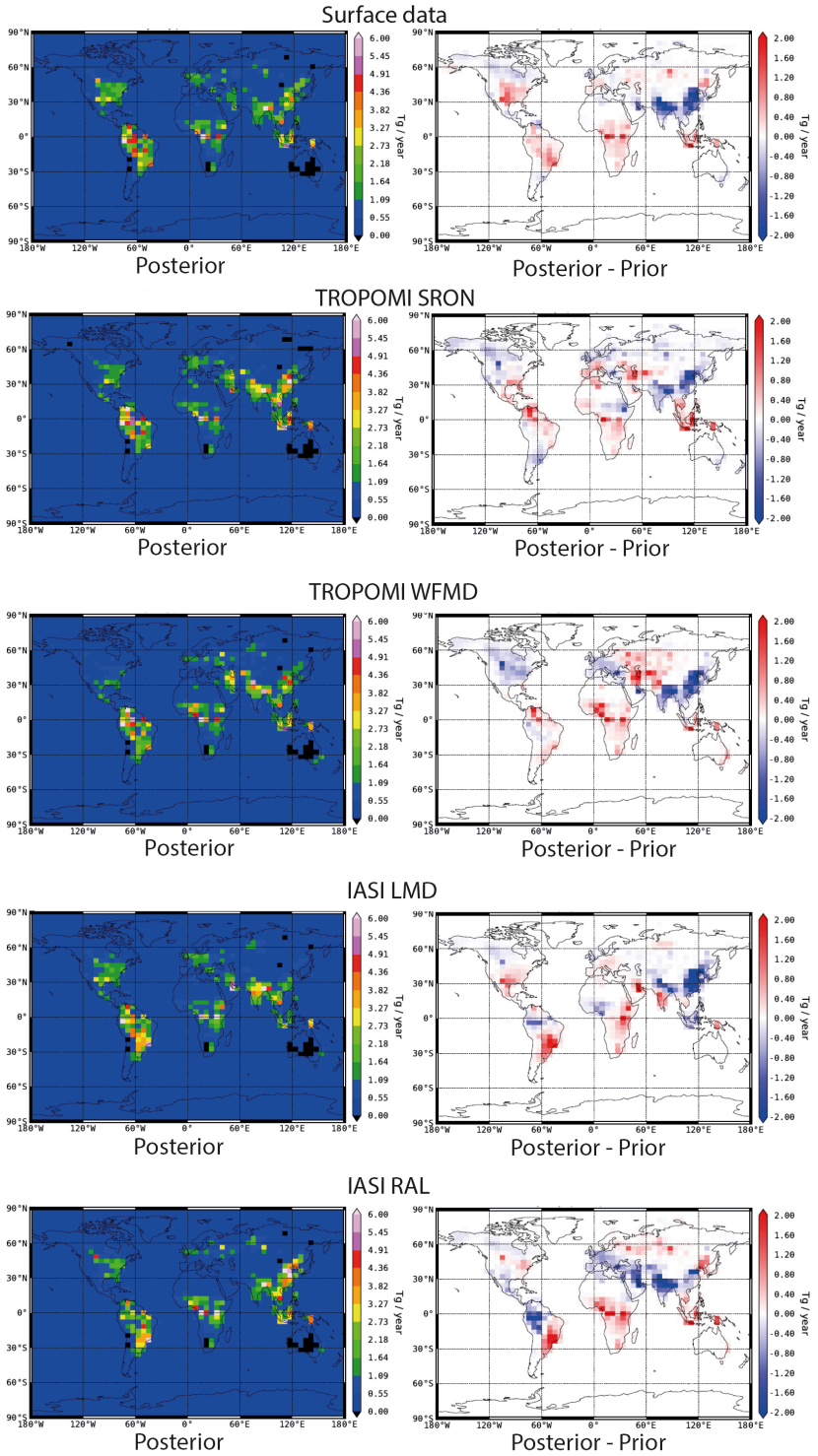

Figure 11: TM5-4DVAR optimized fluxes (left panels) and differences with the prior fluxes (right panels) for inversions using different satellite datasets. The fluxes represent the 2-year period of 2018-05-01 until 2020-05-01.

The inversions using Tropomi and surface data increase the emissions over tropical land (Indonesia, Tropical Africa, Tropical South America). This is less clear in the IASI inversions, which do not agree in the distribution between the three continents. Results for Europe and the USA are quite variable among all inversions. Note that the 2-year TM5-4DVAR inversions do not optimize the OH sink.

4.1.2. Jena CarboScope (DLR)

For the Jena CarboScope, we begin by taking a look at the spatial patterns in the posterior fluxes, as well as the increment from the prior, for different satellite datasets. These results are shown in Figure 12. This is similar to Figure 11 for TM5-4DVAR, though the datasets do not exactly overlap. Furthermore, the two-year period shown here is from 1 January, 2019 to the end of December, 2020.
Comparing across datasets, and between inversion systems, it can be seen that there are some similarities in terms of spatial patterns. The surface inversion with the CarboScope also show negative increments (a reduction in emissions) over China, as was seen in the TM5-4DVAR runs. This pattern is not as robustly visible in the other simulations however, with the exception of the WFMD inversion.
The flux increments across south America are broadly similar across all the remote sensing products, but are both smaller and differently distributed for the surface-based inversion. In this regard, the surface-based inversion with the Jena CarboScope.
Unsurprisingly, the extremely large model-data mismatch found between the surface-optimized fields and the RAL IASI retrievals (second from the bottom) result in unrealistically large increments. This result can only be interpreted as a failure of the model to represent and interpret the measured gradients in the upper-troposphere-lower-stratosphere.
The poor performance of the IASI total column product makes the comparatively reasonable results from the 0-6 km sub-column from the joint SWIR-TIR retrieval all the more interesting. The spatial patterns in the resulting flux increments are rather consistent with those seen in the SRON retrieval, and the WFMD retrieval. Whether that is simply reflecting the information content of the SWIR columns in this joint product or rather improved information about the lower troposphere remains a topic for investigation.
Finally, the inversion results when using the two different methods of bias correction were round to be remarkably similar. This is somewhat surprising, given the difference in their structure, but also reassuring. While the results of Figure 10 clearly show that applying some bias correction is helpful, the differences between the two approaches do not seem to result in significant differences in the resulting fields.

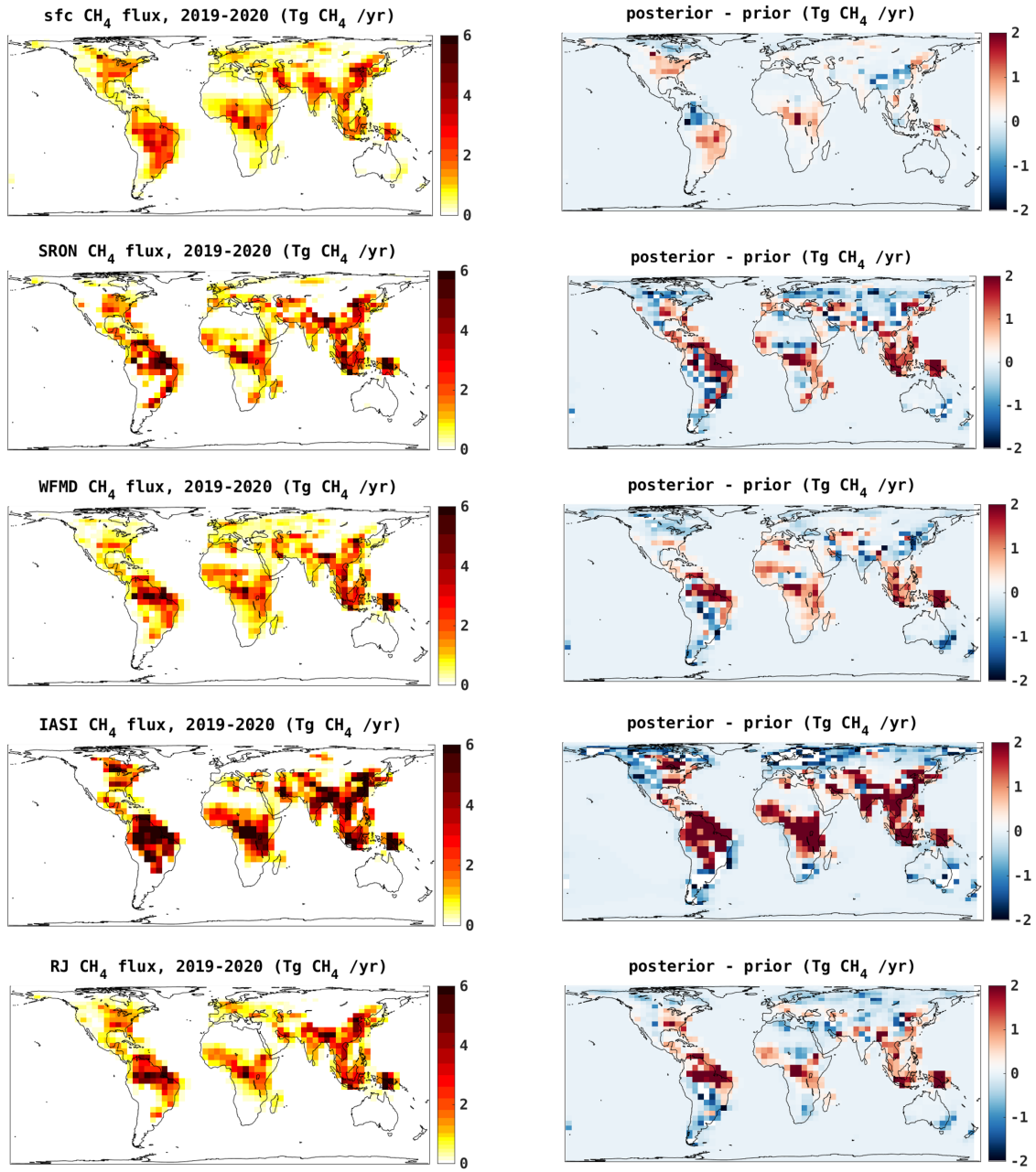

Figure 12: Posterior annual fluxes, averaged over 2019-2020, are shown on the left. The increment (posterior - prior) is shown on the right. From the top, the datasets used are: surface stations, SRONv17, WFMDv1.5, IASI-RAL, and the joint SWIR-TIR retrieval from RAL (labelled RJ for "RAL-Joint").

4.2. The combined use of TROPOMI and IASI data

In this section, we explore the combined use of TROPOMI and IASI data in inversions with and without the optimization of sinks. All these inversions have been performed for the 3-year time window.

4.2.1. Fit residuals: SWIR-TIR vs single instrument inversions

Before assessing the impact of the combined use of IASI and TROPOMI data on the estimated fluxes, we first assess the inversion performance following the same procedure as used in section 3 for the 2-year TM5-4DVAR inversions.
Fit residuals for 3-year inversions using either TROPOMI or IASI data, with and without OH optimization, are shown in Figure 13. The results look very similar to what was found in the 2-year inversions, with very minor differences between inversions that optimize OH or not. The fit residuals for inversion that combines TROPOMI and IASI data, shown in Figure 14, shows systematic deviation of a few ppb in the Tropics, with the optimized model being higher than the combined TROPOMI and IASI data.
The joint SWIR-TIR retrieval for 0-6 km shows significantly deteriorated residuals compared with the other inversions, reflected also in standard deviations that are about twice as large. Larger differences are found *a priori* as well as *a posteriori*, indicating that the prior model is further away from these data and that the inversion has only a limited ability to repair the problem. The posterior solution does reduce the systematic high bias compared with the observations but has difficulty fitting the variation within the hemispheres, particularly towards the poles.

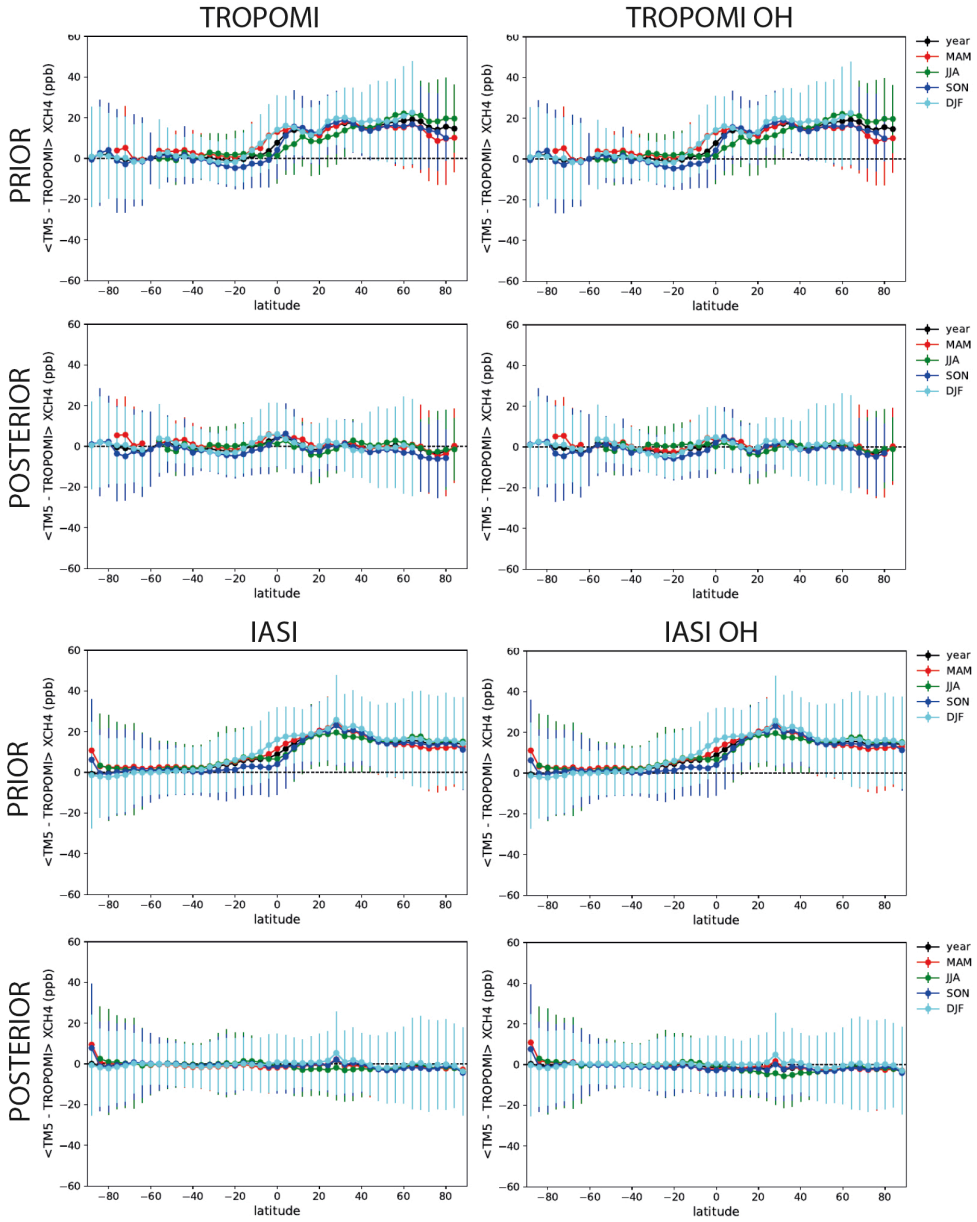

Figure 13: Comparison of zonal and seasonal mean fit residuals between TM5-4DVAR before (prior) and after (posterior) inversion optimization for 3-year inversions. Error bars represent the standard deviation of the variation within each latitude bin.

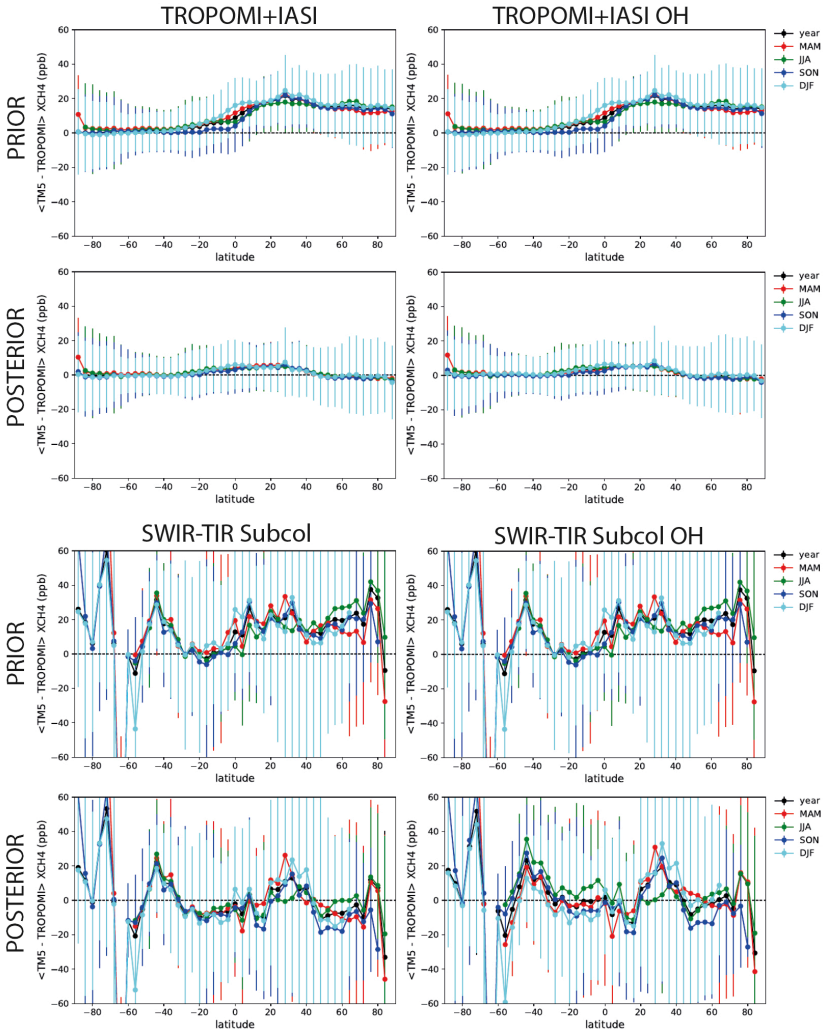

Figure 14: As Figure 13 for the combined use of TROPOMI and IASI data.

The reduced performance of the join SWIR-TIR inversion is confirmed in the comparison to surface measurements (Figure 15). The cause of this is currently not clear. We were glad to be able to make a first attempt at inverting this data product within the timeframe of the Methane+ project, but the results call for a more detailed analysis of possible causes (e.g. problems with the implementation of the averaging kernel, data filtering) than we were able to do.

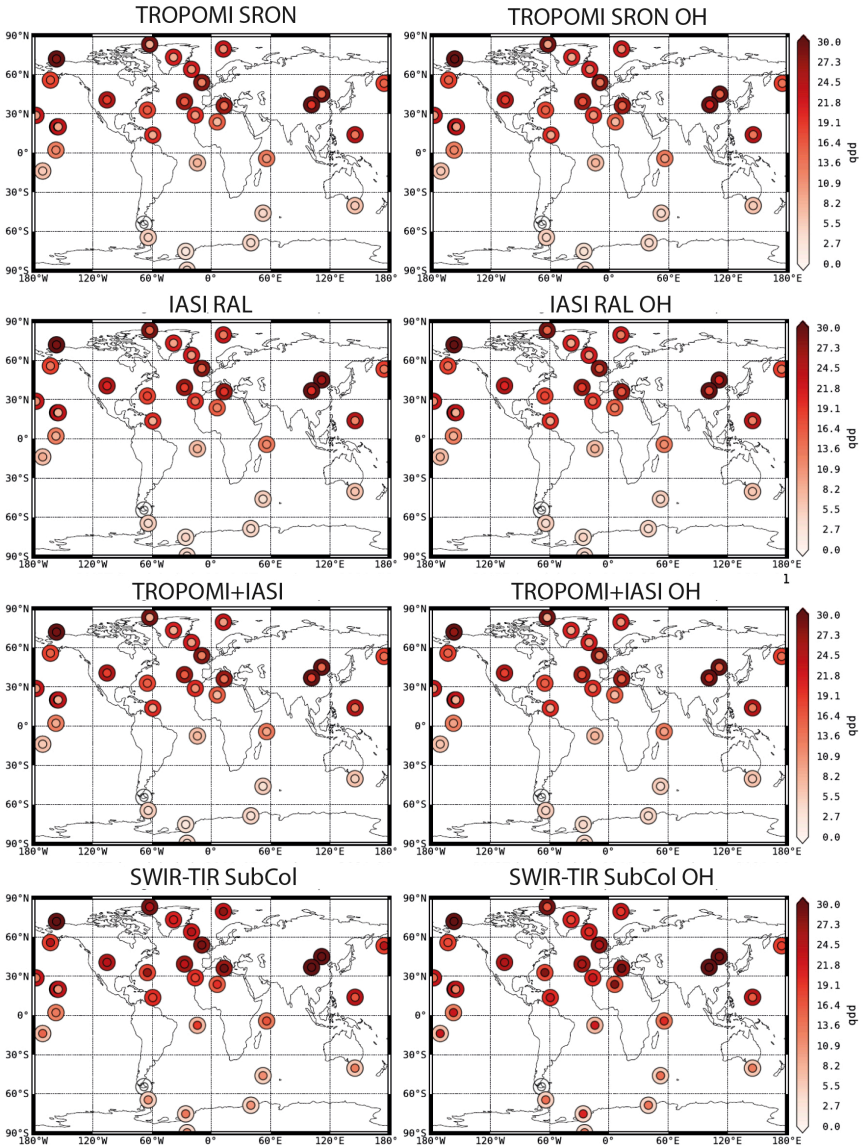

Figure 15: Fit residuals between TM5 and surface measurements for 3-year inversions. Outer rings represent the RMSE between measurements and the *a priori* model, inner circles that of measurements and the *a posteriori* model.

4.2.2. Comparison of 3-year inversions in TM5-4DVAR

In this section we examine the results of the 3-year inversions, focusing on the difference between the flux estimates for 2020 and 2019. The estimated global totals vary substantially between inversions that use different satellite datasets (see Table 3.1). *A priori* emissions are 11 Tg/yr lower for 2020 than for 2019, which can be explained by the reduced economic activity and associated reductions in the demand for oil, coal, and gas during the Covid-19 pandemic. To fit the observed growth rate acceleration in 2020 of about 5 ppb/yr (as reported by NOAA), the inversion can either increase the emissions, decrease OH, or do a combination of the two. As seen in Table

2, solutions are found using different satellite datasets that do not agree with any of these scenarios.

Without OH optimization, *a posteriori* emissions increase between 20 and 25 Tg/yr, except for the IASI RAL inversion which increases the emissions by only 7 Tg/yr. With OH optimization, the surface inversion balances this mismatch largely with a decrease in the sink. Other inversions, again with the exception of IASI RAL, find solutions that increase rather than decrease OH. Such solutions can increase the methane burden if the emissions increase even more, which is indeed what happens. The TROPOMI SRON inversion with OH optimization increases emissions by 55 Tg/yr (30 Tg/yr emission more than without OH optimization), while OH is increased by 8%. The extension of this inversion with IASI data in the TROPOMI+IASI inversions bring this solution into a more realistic range of a 33 Tg/yr emission increase in combination with a 5% increase in OH.

Table 2: TM5-4DVAR estimated global source and sink differences between 2020 and 2019.

Inversion	Δ Global emission (Tg/yr)[#]	Δ OH sink (%)[#]
A priori	-11	0
Surface data	-4 (20)[$]	-8 (0)[$]
TROPOMI SRON	55 (25)	8 (0)
IASI RAL	6 (7)	-2 (0)
TROPOMI+IASI	33 (20)	5 (0)
Joint SWIR-TIR 0-6km	73 (22)	3 (0)

[#]: 2020 minus 2019; [$]: Results in parentheses are for inversions that do not optimize OH.

To understand what might cause the varying solutions and increases in OH that seem inconsistent with an enhanced growth rate, we need to examine the spatial patterns of emission adjustment (see the right most column of Figure 12). The largest emission increases are found in the northern-hemisphere Tropics. Depending on the sign of the OH adjustment, this increase is large or small.

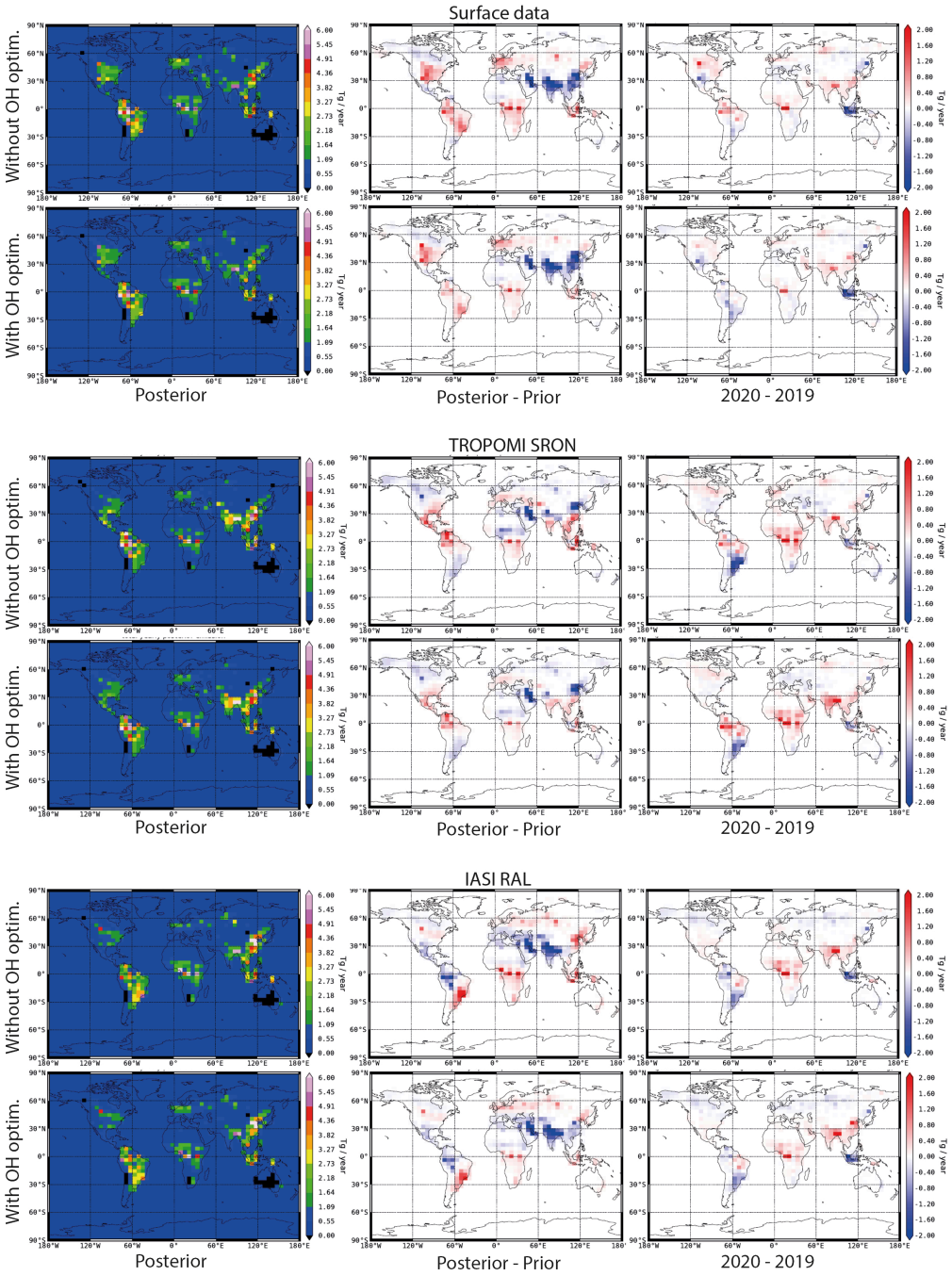

Figure 16: TM5-4DVAR optimized fluxes (left panels), differences with the prior fluxes (middle panels), and difference between posterior fluxes for 2020 and 2019 (right panels) for inversions using different satellite datasets. The fluxes represent the 2-year period from 2019-01-01 until 2021-01-01.

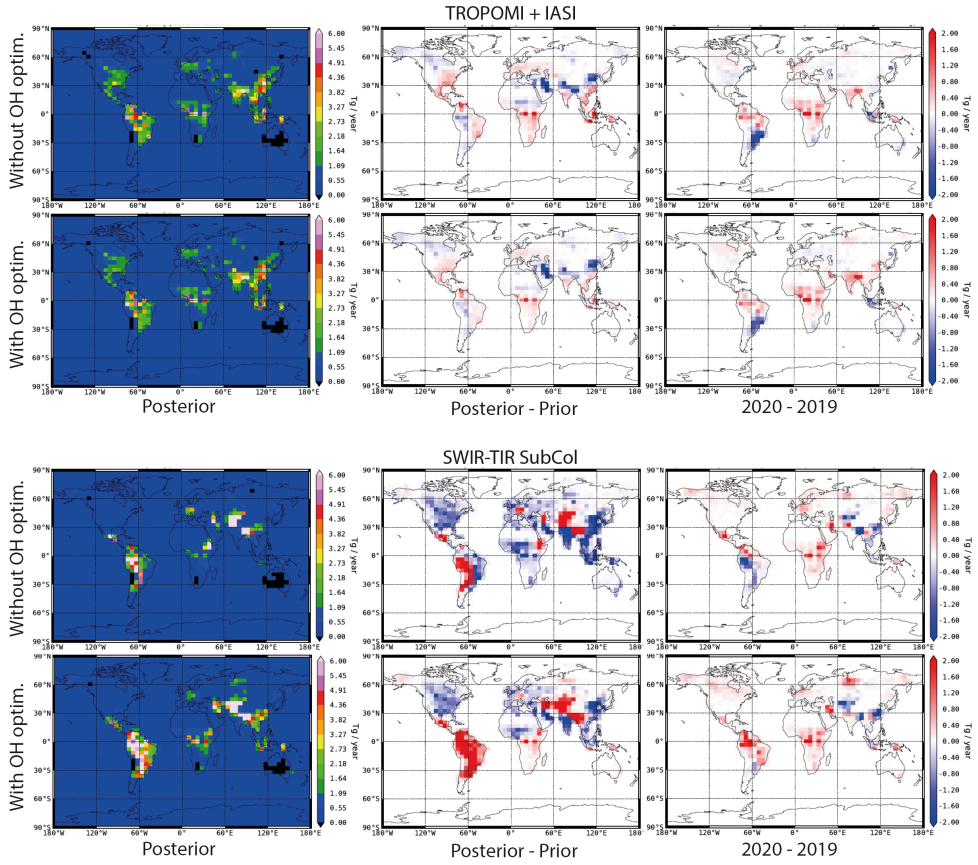

Figure 17: As Figure 16 for inversions combining data from TROPOMI and IASI.

The location coincides with the latitudinal band where the largest impact of OH changes are expected. This is because OH levels are highest in the Tropics and because the Northern hemisphere is most strongly influenced by anthropogenic emissions of air pollutants, and therefore by reduced emissions during COVID lockdowns. The trade-off between emission and sink adjustments in the inversion is probably driven by differences in the degrees of freedom that are assigned to them in the inversion setup. Since the OH field is only adjusted by a global and annual scaling factor, there is no flexibility to adjust OH only in the Northern Hemisphere Tropics. Depending on the strength of the observational constraint on changes in this latitudinal zone, emission adjustments might be more effective than sink adjustments. To investigate if this mechanism could lead to the misattribution of a sink to a source, additional inversions would be needed in which the number of degrees of freedom of the sink is varied.

4.2.3. Regional benefits of joint SWIR-TIR retrievals

Three regional cases have been analyzed in further detail to investigate the added value of combining SWIR and TIR retrievals. These are cases where information about the vertical profile of methane is expected to matter for a correct source attribution.
The first case is the Indian summer monsoon, which injects a large amount of methane from low elevations into the free troposphere south of the Himalayas. In the upper troposphere, this methane is further transported by eastward and westward branches of the monsoonal circulation, respectively towards China and the Middle East. If only total column information is available, then methane enhancements over China and the Middle East originating from India could be misattributed to regional emissions by the inversion. Combining TROPOMI and IASI data could avoid this misattribution by constraining the contributions of the lower and upper troposphere to the total column.

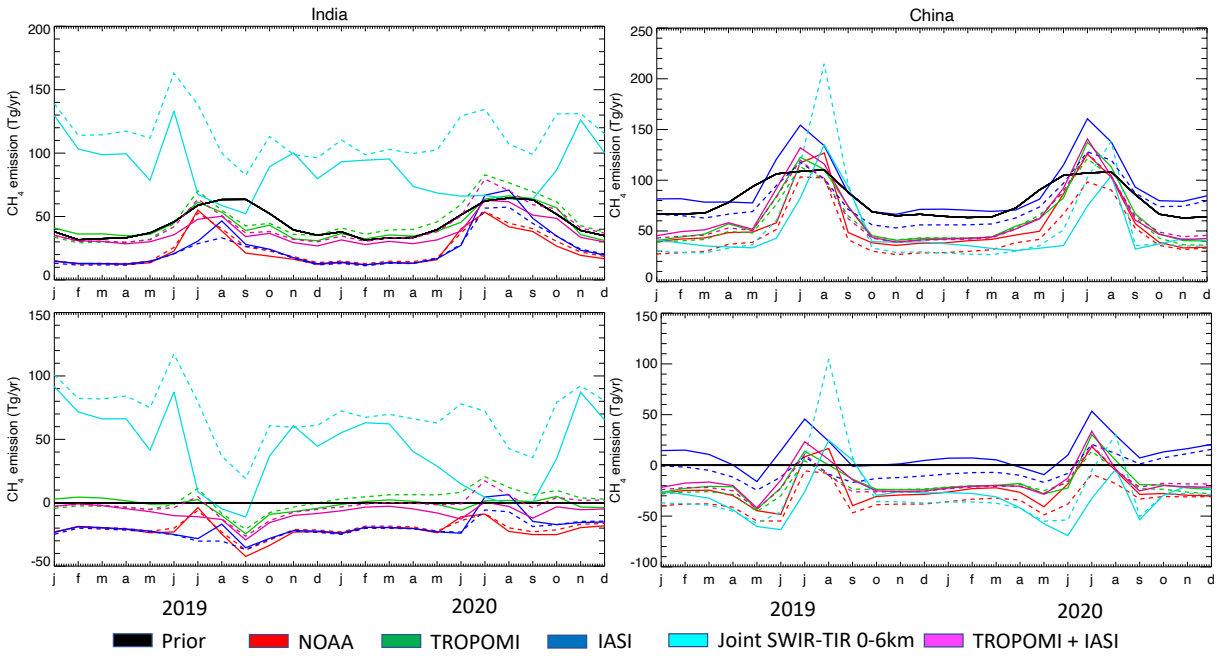

Figure 18: Region integrated fluxes over India and China. Dashed lines represent inversions that optimize OH. In the bottom panels the prior flux has been subtracted.

Monthly methane emission from TM5-4DVAR integrated over India and China are shown in Figure 18 for the 3-year inversions. On average, TM5-4DVAR reduces emissions over India and China compared with the prior. During the summer monsoon, Chinese emissions are overestimated and Indian emission are underestimated compared with the prior, which is consistent with a transport-induced misattribution of emissions. Surprisingly enough, the inversion using IASI data, which mostly address the free troposphere, shows this most strongly. The TROPOMI inversion stays closest to the prior for India, and close to the prior of China also during the monsoon season. Combining IASI and TROPOMI data in a single inversion yields a solution that is closest to the use of TROPOMI only. Hence, it can be concluded that the emission attribution to China and India is sensitive to the dataset that is inverted. It is not clear,

however, if the use of IASI data, either alone or in combination with TROPOMI, improves the regional emission attribution.

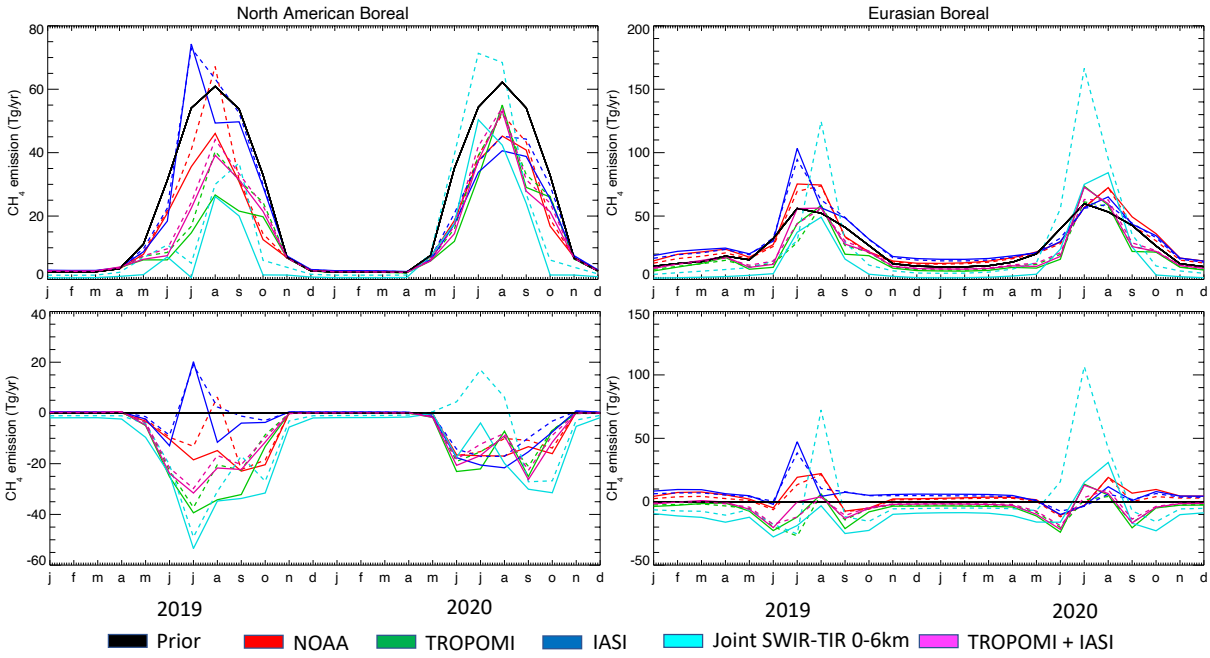

Figure 19: Region integrated fluxes over the northern high-latitudes. Dashed lines represent inversions that optimize OH. In the bottom panels the prior flux has been subtracted.

The second case investigates whether inversion-estimated methane emissions from high-northern latitudes are sensitive to the extended seasonal coverage of the high-latitudes provided by IASI in comparison to TROPOMI. Emissions are presented (see Figure 19) for Transcom regions North American Boreal, including Canada and Alaska, and Eurasian Boreal, covering the boreal/arctic zone of Eurasia east of the Ural Mountains. On average, the inversions reduce emissions over North America and increase emissions over Asia compared with the prior. All inversions agree on very low wintertime emissions over North America. Wintertime emissions are higher over Asia and highest using IASI data. Here the inversion using TROPOMI and IASI is more strongly influenced by IASI then in the previous example. This makes sense, considering the year around availability of IASI data. The range of emission estimates is widest during summer – when observational constraints are strongest, but a priori flux uncertainties are also largest.

The last case is chosen over Tropical Africa and South America, where the XCH4 seasonality is driven by emissions from tropical wetlands and the movement of the Inter Tropical Conference Zone (ITCZ). Again, the combination of TROPOMI and IASI could, in theory, facilitate the correct attribution of large-scale circulation (dominant at higher elevation) and regional emissions (dominant near the surface). The inversion estimated fluxes (see Figure 20) show increased emissions compared with the prior over equatorial Africa with the largest emissions from the NOAA and IASI inversions. Using TROPOMI, the emissions are least enhanced (disregarding the joint SWIR-TIR

inversion). As for India and China, the impact of low vs high elevation retrieval sensitivity is opposite to the expectation. As expected, again, the inversion using IASI and TROPOMI data is in between the inversions using each of them. Over Tropical South America, the IASI emission are lowest (and lower than the prior). Here, however, the deviations from the prior are not as strong – in a relative sense – as over equatorial Africa.

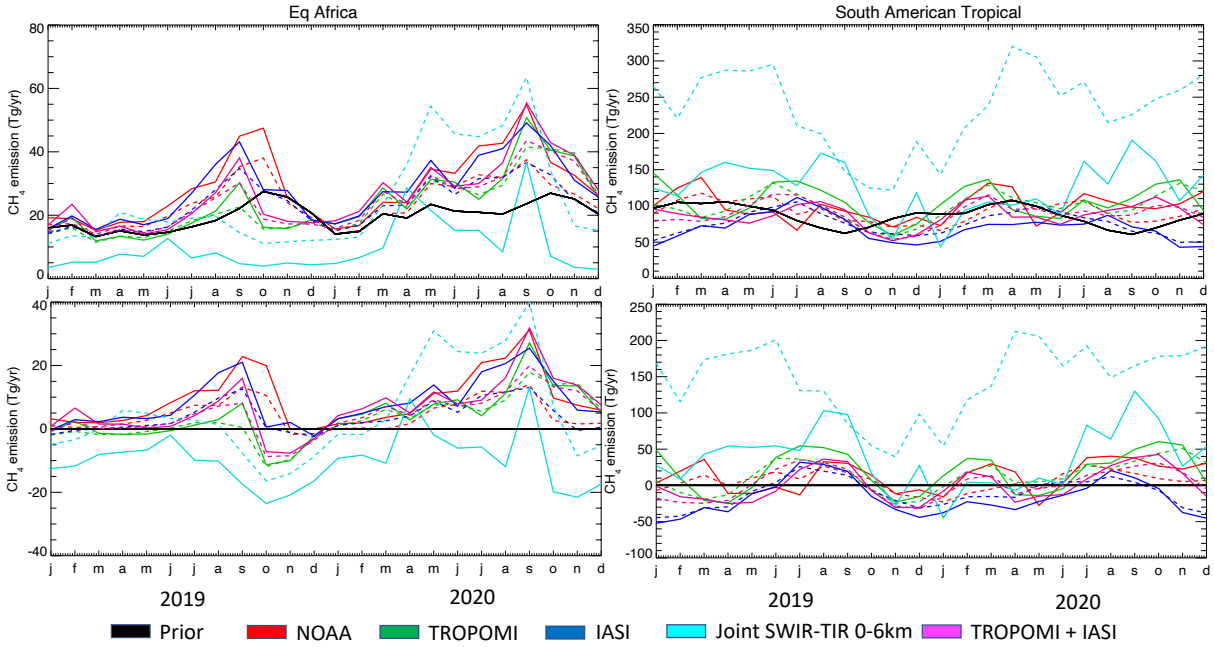

Figure 20: Region integrated fluxes over the Tropical rainforests. Dashed lines represent inversions that optimize OH. In the bottom panels the prior flux has been subtracted.

4.3. Validation with independend measurements

4.3.1. TM5-4DVAR

Output of TM5-4DVAR has been compared to TCCON measurements (Figure 21). In this comparison, the TCCON averaging kernel has been applied to the modelled vertical profile using equation 2 applied to TCCON kernels and a priori profiles. The bias corrections have been added to the modelled total columns. This way the model would be in agreement with TCCON if it exactly reproduced the satellite data, accounting for the mean bias, and the satellite data would exactly agree with TCCON. As seen in Figure 21, the optimized fits to satellite data reduce the bias with TCCON. However, offsets remain, most notably at sites in the Southern Hemisphere. These offsets are not explained by the satellite data themselves, which generally do not show such biases compared with the GGG2014 TCCON data that have been used here.

The only explanation is that the limited number of TCCON sites is not representative of the hemispheric mean.

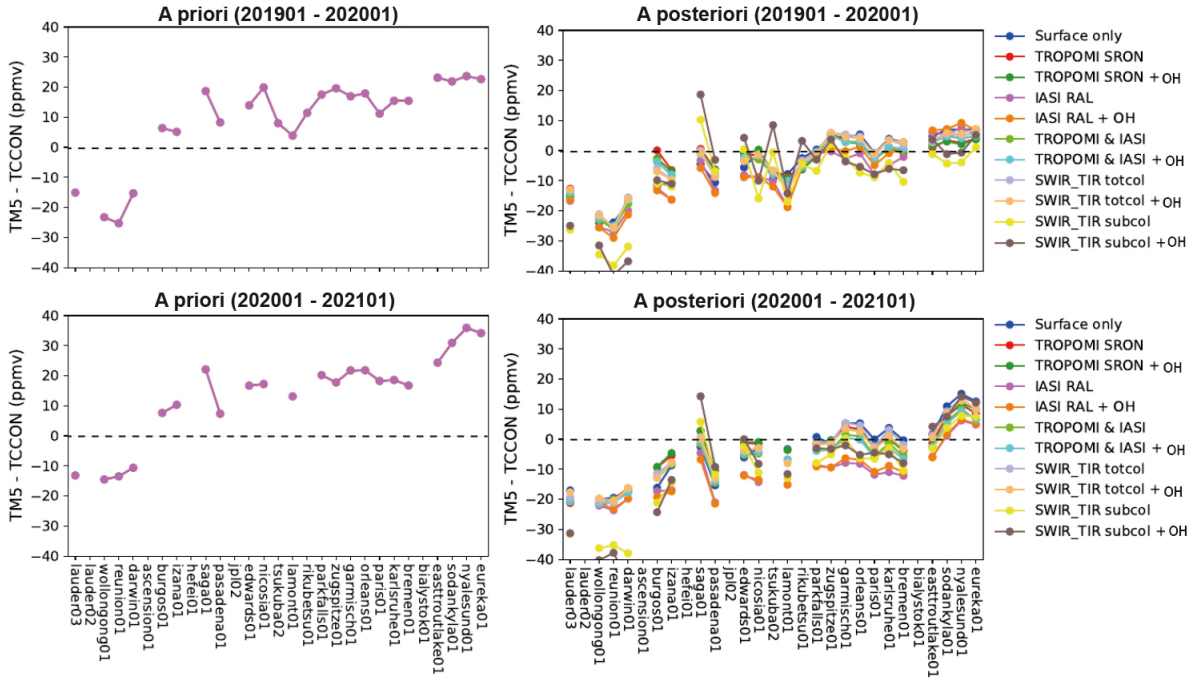

Figure 21: TM5-4DVAR Comparison to TCCON.

4.3.2. Jena CarboScope (DLR)

A similar comparison to that in Figure 21 has been carried out for the Jena CarboScope inversion. This is shown in Figure 22. Compared to similar comparisons carried out with the last generation of satellite products, the agreement is substantially worse, which is quite surprising. Indeed, most of the satellite products appear to be biased low with respect to the TCCON measurements. A potential contributing factor to this is the use of a brand-new data release from TCCON, GGG2020, in which many of the variables have been renamed, and units have been changed. It is possible that the wet-air/dry-air correction has thus not been applied properly. This remains to be addressed.

Another data source that can be used for analysis of the optimized concentration fields is aircraft measurements. Several sources of data were collected for this analysis, including regular NOAA profiles from a recent ObsPack data release (Schuldt et al., obspack_ch4_1_GLOBALVIEWplus_v4.0_2021-10-14), one ATom campaign from 2018, and all of the available IAGOS flights over the study period (Petzold et al., 2015; Filges et al., 2015).

A first look at these data is provided in Figure 23. At first glance it is not clear if either the (co-)assimilation of TIR data or the inclusion of OH optimization substantially improves the performance. More analysis of the spatial biases (particularly for the

global datasets IAGOS and ATom is foreseen. At present no bias correction has been applied (or removed) when comparing the posterior fields with the measurements, but this may also be worth reconsidering.

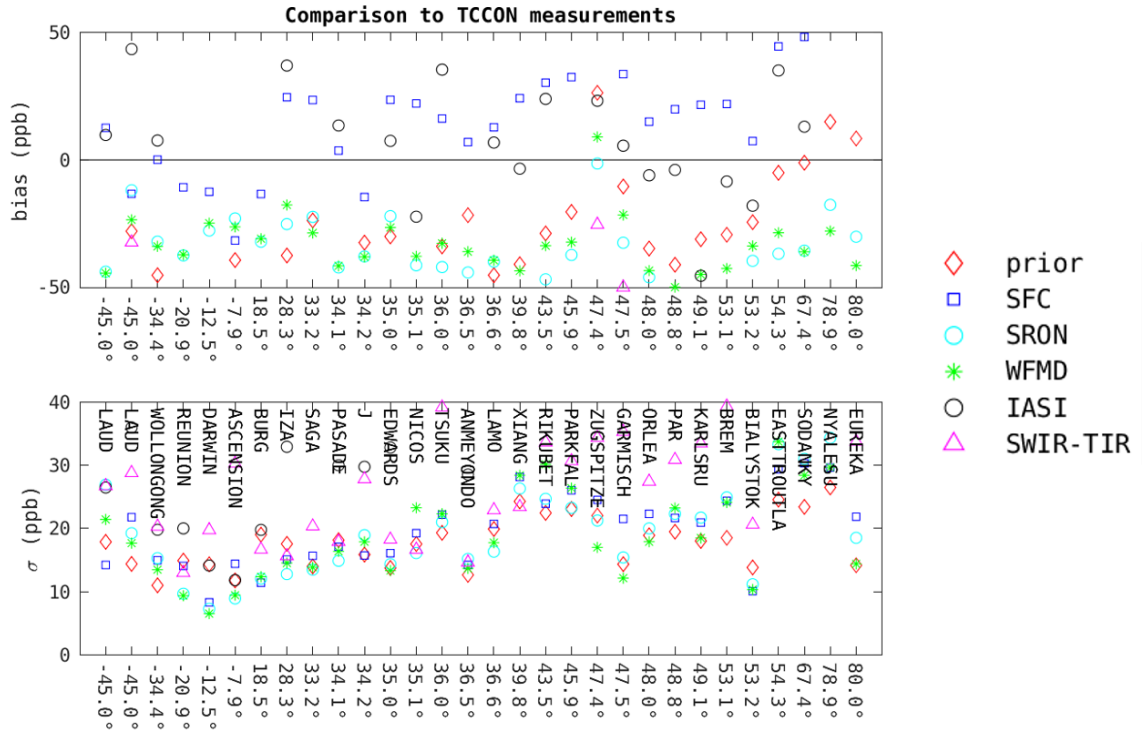

Figure 22: Comparison between TCCON measurements and various inversions carried out with the Jena CarboScope. The top panel shows mean bias per station, and the bottom panel shows the standard deviation of the difference.

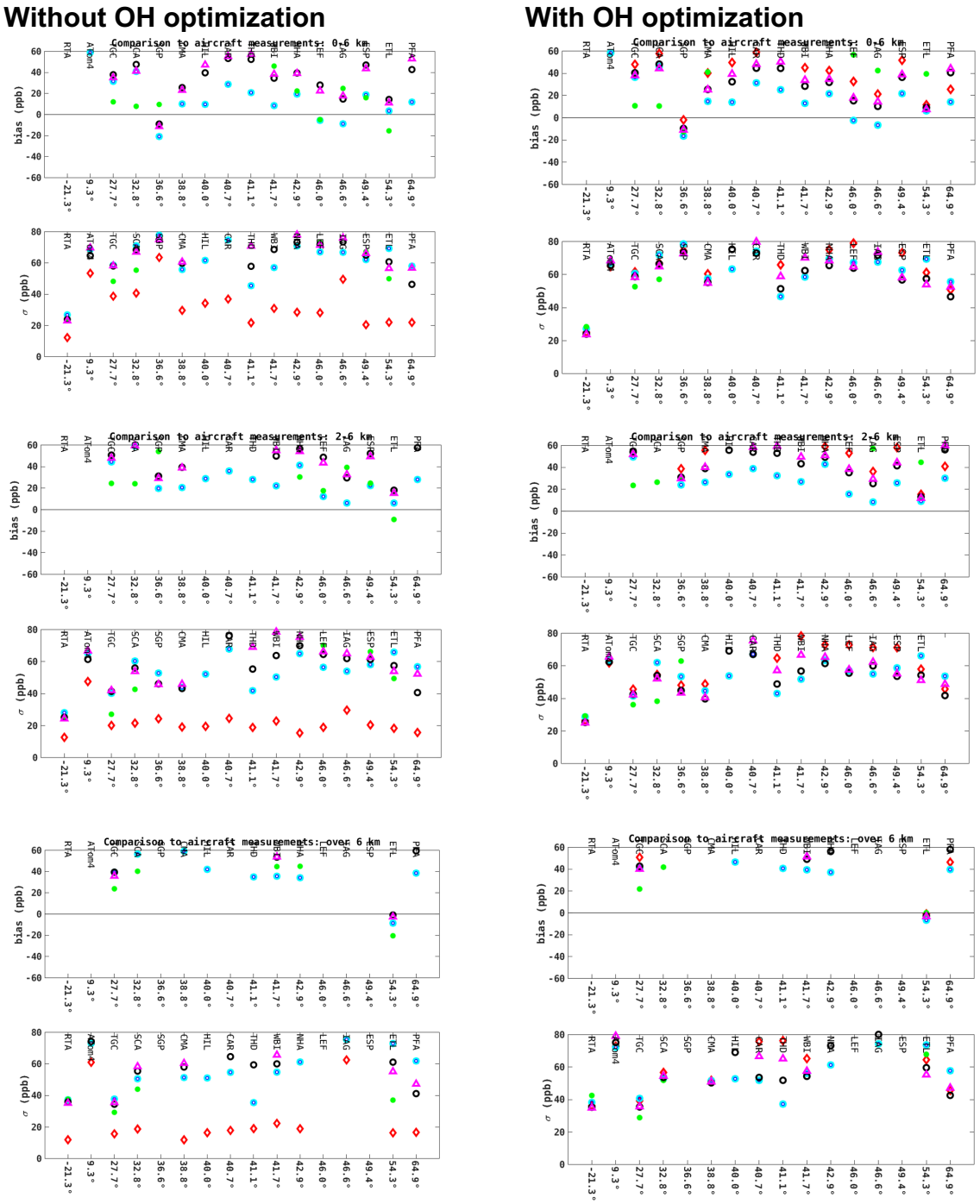

Figure 23: As for Figure 22, but with comparison against aircraft data. The left column is without OH optimization, and the right is with OH optimization. The top panels show all data between 0-6 km, the center panels show data between 2-6 km, and the lowermost panels show only data above 6 km.

5. Summary and recommendation for future work

This report documents the inversion setup-ups that were developed in the Methane+ project to make use of the retrieval datasets of total column methane from TROPOMI and IASI that were made available from WP2000, and the inversion results that have been obtained using these datasets. This is done for the TM5-4DVAR and Jena CarboScope inversion systems, that are compared and evaluated using independent aircraft data. In addition to reading and processing the satellite data such that consistent comparisons can be made between satellite data and atmospheric transport model output, taking their respective uncertainties into account as well as possible, we also extended the control vector of the TM5-4DVAR system with additional degrees of freedom to allow optimization of methane sinks.

The results confirm that our setups succeed in fitting the satellite datasets such that the consistency with the surface network is maintained. This is true for all retrieval datasets, including an inversion setup which combines TROPOMI and IASI data, but excluding the use of 0-6 km sub columns from the joint SWIR-TIR retrieval. The reason why the TM5-4DVAR inversion had difficulty fitting these data has not been elucidated yet. The combined use of IASI and TROPOMI data to constrain a tropospheric sub-column is a promising approach because it should reduce or eliminate biases introduced by inconsistencies in the representation of the stratospheric sub-column. Therefore, it is recommended to continue the development of this retrieval product and its use in inversions, to solve the remaining issues.

Our inversions have been extended by one year beyond the 2-year period that was proposed initially, to explore the use of the new satellite data to investigate the sharp rise in global CH_4 that has been observed in 2020, and continued during 2021. The difference between optimized fluxes for 2019 and 2020 points to the northern hemisphere tropics as having the largest contribution to this increase. Whether emissions increased or atmospheric sinks decreased cannot unambiguously be concluded from our inversions, as their relative contributions are sensitive to the dataset that is used.

So far, sinks have only been optimized using a single global and annual scaling factor. If global CH_4 sinks changed significantly due to changing emissions of photochemically reactive precursors of OH, such as NO_x, during COVID lockdowns, then this OH change is likely to have varied globally. In this case, additional degrees of freedom would be needed in the inversion to account for such changes. How to balance the degrees of freedom assigned to global methane sources and sink is a difficult question that requires further research. An easy next step would make use of output of CTM simulations that attempt to represent the change in OH. These OH fields could be optimized further or used to guide the choice of additional degrees of freedom for optimizing OH.

To further investigate the added value of combining SWIR and TIR data, our analysis focused on regions where the vertical distribution of methane could be critical for a correct regional attribution of emissions. This was investigated for the influence of the Indian monsoon on inversion-estimated emissions from China and India, the influence

and the seasonal migration of the ITCZ on the seasonality of emissions from tropical wetlands, and the seasonality of emissions at high northern latitudes. In the latter case, the advantage of combining SWIR and TIR lies mostly in the extended seasonal data coverage that TIR data can bring at high latitudes. The results of these regional analyses confirm that the optimized emissions are sensitive to the satellite dataset that is used. The combined use of SWIR and TIR data leads to solutions that are in between those of the separate datasets, with a balance between the two that can be explained by the weights of the constraints imposed by each of them. However, whether or not the use of more data leads to more realistic solutions cannot be concluded from the results that were obtained. It would require extended validation using independent measurements, which is also a recommended next step.

6. References

Filges, A., C. Gerbig, H. Chen, H. Franke, C. Klaus, and A. Jordan. “The IAGOS-Core Greenhouse Gas Package: A Measurement System for Continuous Airborne Observations of CO2, CH4 , H2O and CO.” Tellus B 67 (January 1, 2015). https://doi.org/10.3402/tellusb.v67.27989.

Hasekamp, O., Lorente, A., Hu, H., Butz, A., aan de Brugh, J., and Landgraf, J.: Algorithm Theoretical Baseline Document for Sentinel-5 Precursor methane retrieval, available at: http://www.tropomi.eu/documents/atbd/ (last access: 11 January 2021), 2019

Locatelli, R., Bousquet, P., Saunois, M., Chevallier, F., & Cressot, C. (2015). Sensitivity of the recent methane budget to LMDz sub-grid-scale physical parameterizations. *Atmospheric Chemistry and Physics*, *15*, 9765–9780. https://doi.org/10.5194/acp-15-9765-2015

Monteil, G., Houweling, S., Guerlet, S., Schepers, D., Frankenberg, C., Scheepmaker, R., Aben, I., Butz, A., Hasekamp, O., Landgraf, J., Wofsy, S. C., & Röckmann, T. (2013). Intercomparison of 15 months inversions of GOSAT and SCIAMACHY CH4 retrievals. 118, 11807, doi:10.1002/2013JD019760.

Petzold, A., V. Thouret, C. Gerbig, A. Zahn, C. Brenninkmeijer, M. Gallagher, M. Hermann, et al. “Global-Scale Atmosphere Monitoring by in-Service Aircraft - Current Achievements and Future Prospects of the European Research Infrastructure IAGOS.” Tellus B 67 (January 1, 2015). https://doi.org/10.3402/tellusb.v67.28452.

Schuldt, K. N., T. Aalto, A. Andrews, S. Aoki, J. Arduini, B. Baier, P. Bergamaschi, et al. (2021): Multi-laboratory compilation of atmospheric methane data for the period 1983-2020; obspack_ch4_1_GLOBALVIEWplus_v4.0_2021-10-14; NOAA Earth System Research Laboratory, Global Monitoring Laboratory. http://doi.org/10.25925/20211001.

Segers, A. and S. Houweling, 2020, Description of the CH4 Inversion Production Chain, Copernicus Atmosphere Monitoring Service, https://atmosphere.copernicus.eu/sites/default/files/2020-01/CAMS73_2018SC1_D73.5.2.2-2019_202001_production_chain_v1.pdf

Total Carbon Column Observing Network (TCCON) Team. (2022). *2020 TCCON Data Release* (Version GGG2020) [Data set]. CaltechDATA. https://doi.org/10.14291/TCCON.GGG2020

***** End of Document *****